Integrated patch and slot array antenna for terahertz quantum cascade lasers at 4.7 THz

C. Bonzon,[a] I. C. Benea Chelmus, K. Ohtani, M. Geiser, M. Beck, and J. Faist
Institute for Quantum Electronics, ETH-Zürich, CH-8093 Zürich, Switzerland

(Received 15 January 2014; accepted 31 March 2014; published online 21 April 2014)

Our work presents a slot and a patch array antenna at the front facet of a 4.7 THz quantum cascade laser as extractor, decreasing the facet reflectivity down to 2.6%. The resulting output power increases by a factor 2 and the slope efficiency by a factor 4. The simulated and the measured far-fields are in good agreement. © *2014 AIP Publishing LLC*. [http://dx.doi.org/10.1063/1.4871369]

Nowadays, quantum cascade lasers (QCLs)[1] are among the best sources of terahertz radiation[2] due to their compactness and wide range of available lasing frequencies. They reach the milliwatt level in output power from roughly 1–5 THz.[3–5] Their largest drawback however remains the maximum operation temperature. The current best performance is based on dry etched double metal waveguides[6] ensuring a good heat dissipation and a homogeneous electron injection due to vertical sidewalls. Narrow 3rd order distributed feedback lasers (DFBs) have shown a high temperature continuous wave (CW) operation and a narrow far-field with single mode emission,[7] but they are inherently single mode sources. The potential of long Fabry-Perot devices cannot be fully exploited, because the mirror losses scale with 1/L and the slope efficiency scales with $\alpha_{rad}/\alpha_{tot}$.[8]

Previous work towards an enhanced broadband extraction studied the addition of a lens, dielectrics,[9,10] or a horn antenna[11] at the front facet of a QCL. These solutions imply often time-consuming manufacturing and are subject to handling errors. At millimeter wavelengths, very low reflectivity transition of the guided wave into free space is achieved with antennas as impedance matching elements. A more recent publication showed the integration of a metamaterial on a double metal ridge[12] as a way of controlling the waveguiding properties as well as the far-field.

As drawn schematically in Figure 1, in this work we propose an approach inspired from the microwave frequency range, a 20 μm wide dry-etched amplifier section is terminated by a Bragg reflector on the front and a patch or slot array on the other. To enhance the outcoupling efficiency,[13,14] the latter were deposited on benzocyclobutene (BCB), a polymer already proven integrable with THz QCL waveguides[15] with a refractive index of 1.55 at 4.7 THz.

The details of the simulation are in the supplementary material[16] and the main results are in Figure 2. The refractive index of BCB was overestimated at the device design so all resonances are blueshifted compared to the active region gain. This value is known to change with processing parameters.[17] All presented simulations in this Letter are done using aforementioned refractive index.

The Bragg reflector (DBR) is composed of a succession of 8 rectangular pillars of 4.5 μm made out of quantum cascade active region spaced by 7 μm of BCB. It is providing a reflectivity of 76% at 4.75 THz in the fundamental mode and is limited by diffraction losses. Mode conversion can be an issue for narrow ridges, in this case 97% of the power is

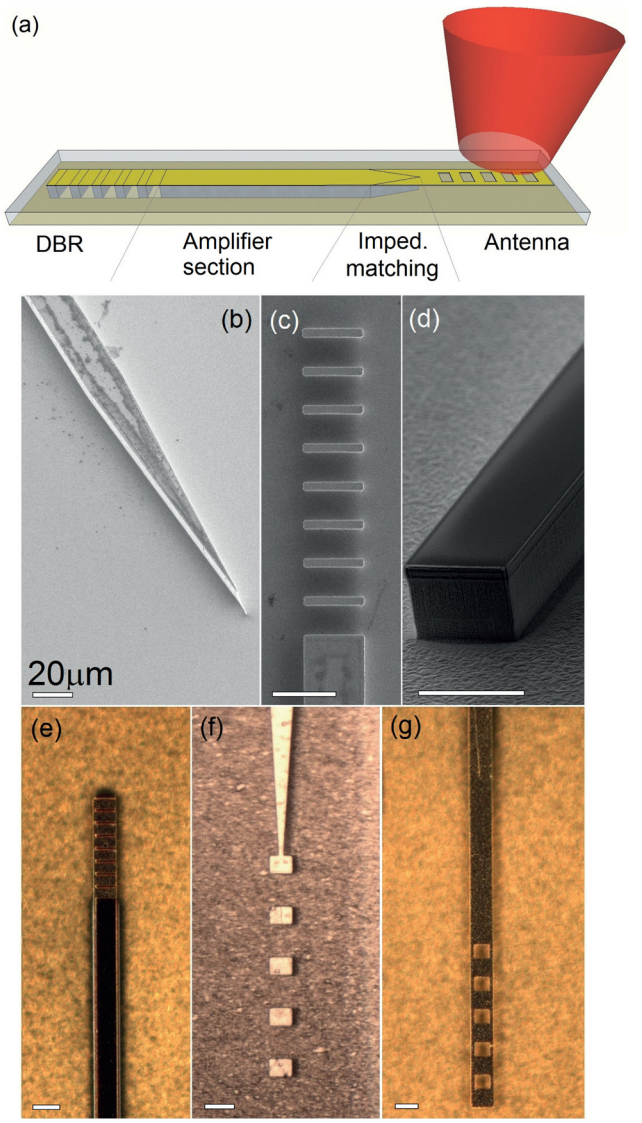

FIG. 1. (a) Schematic of the laser showing the four elements. (b)–(d) SEM pictures of the impedance matching element, the DBR, and the facet of the antennaless device, respectively, these pictures were taken prior to the BCB deposition. (e)–(g) Microscope pictures of the finished elements, the DBR, the patch array antenna, and the slot array antenna, respectively.

[a]bonzonc@phys.ethz.ch

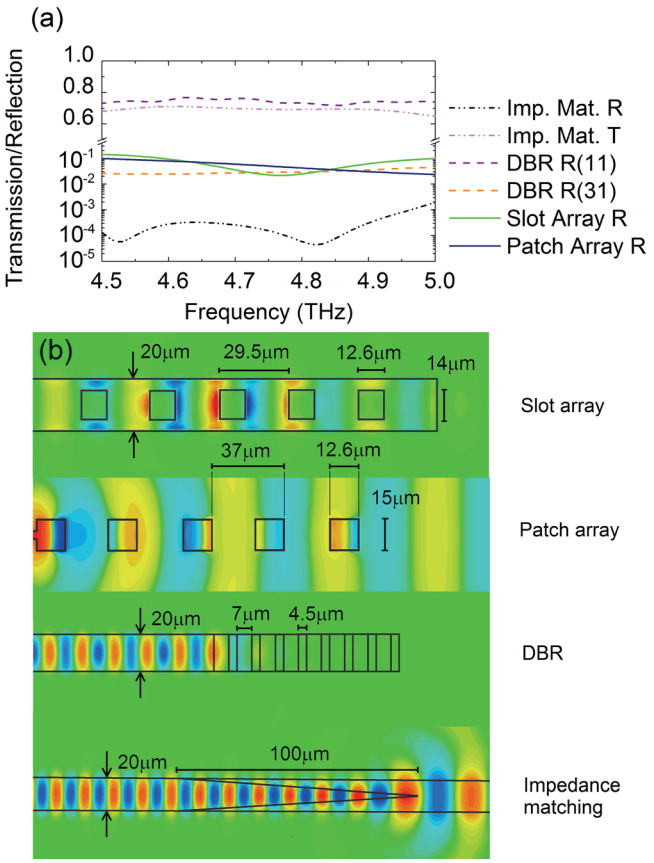

FIG. 2. (a) Computation of the relevant intensity transmission and reflectivity for each element, the scale is first logarithmic from 10^{-5} to 0.4 and then linear from 0.5 to 1. Imp. Mat. R/T is the reflection and transmission for the impedance matching section. DBR R (yx) is the reflectivity of the Bragg reflector in mode y when excited with mode x. (b) Top view of the four elements, showing the out-of-plane electric field plane cut at mid-height between the top and bottom contacts. The field excitation comes from the left at a frequency of 4.75 THz in each case.

reflected in the fundamental mode and the rest in the second excited mode.

An impedance matching element from the amplifier section to the antenna is necessary to avoid any undesired feedback to the amplifier section from the waveguide transition. It consists of a linear tapering of the ridge width from 20 to 0 μm over a 100 μm long distance while keeping the top metallization of constant width. It reflects 0.016% and transmits 70% of the incoming wave intensity. The remaining fraction is scattered out of the waveguide and arises from the non-adiabaticity of the linear tapering close to the impedance matching element tip.

The patch array antenna laser is made of 5 patches of 15 $\times$ 12.6 μm^2 arranged in a linear array of 37 μm period and is implemented with a 2 mm long amplifier section. The first patch antenna is connected to the laser by a BCB microstrip waveguide tapered from 20 to 3 μm over a 155 μm long distance. The antenna shows a reflectivity of 4.8% at 4.75 THz. The electric field of Figure 2(b) shows a single surface plasmon at the bottom gold that couples the patches together, most of the field is extracted by the first patch, the purpose of the others is to enlarge the extraction surface in order to narrow the far-field and to broaden the resonance with respect to the single patch antenna.

The slot array antenna has a complementary geometry to the patch array and is constituted of 5 rectangular holes of 14 $\times$ 12.6 μm^2 in the waveguide in an array of 29.5 μm period and is implemented with a 1 mm long amplifier section. The slot array antenna shows a resonance peaking at 4.78 THz with a minimum of 2.25% reflectivity. The fields show that the five resonators are strongly coupled via the waveguide and result in a overlap of the guided and oscillating fields.

The devices were processed on a 12.5 μm thick four well bound-to-continuum active region grown by molecular beam epitaxy with a resonant phonon injection[18] and a laser transition around 19.4 meV. A gold-gold thermocompressive waferbonding of the layer on a 350 μm GaAs wafer Si-doped at 10^{18} cm^{-3} was realized with Ti/Au of 7 and 500 nm for the bottom contact. After a prior physico-chemical substrate removal, the active region was fully opened and subsequently patterned using inductively coupled plasma etching. The result of this step can be seen in Fig. 1. The structures were then covered with four cycles of CYCLOTENE 3022–57 BCB spinning and baking, reaching an accumulated thickness of about 20 μm and a planar surface. The structures were reopened by removal of the excess polymer by reactive ion etching.[19] At last, the top metal contact and antennas were deposited featuring a thickness of Ti/Au of 7 and 200 nm. SEM pictures revealed that the ridges are 19 μm wide and this value was used for the values of current density.

Devices without antenna were processed for comparison. They are composed of the amplifier section and the DBR. Their facet is thus dry etched and is the interface between the active region and BCB and has a reflectivity of 18%. The linear fit of their measured threshold current as a function of 1/L allows the computation of the waveguide losses[8] using the computed mirror reflectivities. From antennaless devices of lengths 3, 2, 1, 0.5 mm with threshold currents of 202, 240, 257, 353 A/cm^2, the waveguide losses are estimated to 28 cm^{-1}. We attribute the higher observed losses compared to Ref. 20 to the intersubband resonant losses, and the narrow ridge used in the study, as well as the fact that the refractive index of the BCB increases the field at the sidewall location. In addition to providing a single mode operation, the narrow ridge width also provides a better thermal behavior for continuous wave operation.

Figure 3(a) shows the light-current-voltage (LIV) characteristics of an antenna-less against a patch array antenna device. The latter features a fourfold increase in slope efficiency and a doubled peak output power. From the threshold current and the losses mentioned earlier, we deduce a reflectivity of 2.6% from the antenna and impedance adapter which is in good agreement with the predicted value of 2.35%. The main results are summarised in Table I. As already demonstrated,[21] the threshold and the onset of the negative differential resistance current density of the laser reflect the nature of the cavity. As the outcoupling increases, the radiative losses of the cavity increase, resulting in a higher slope efficiency and threshold current density. Additionally, the intracavity field decreases and we see a reduction of the photodriven current and thus a reduction of the onset of the negative differential resistance.

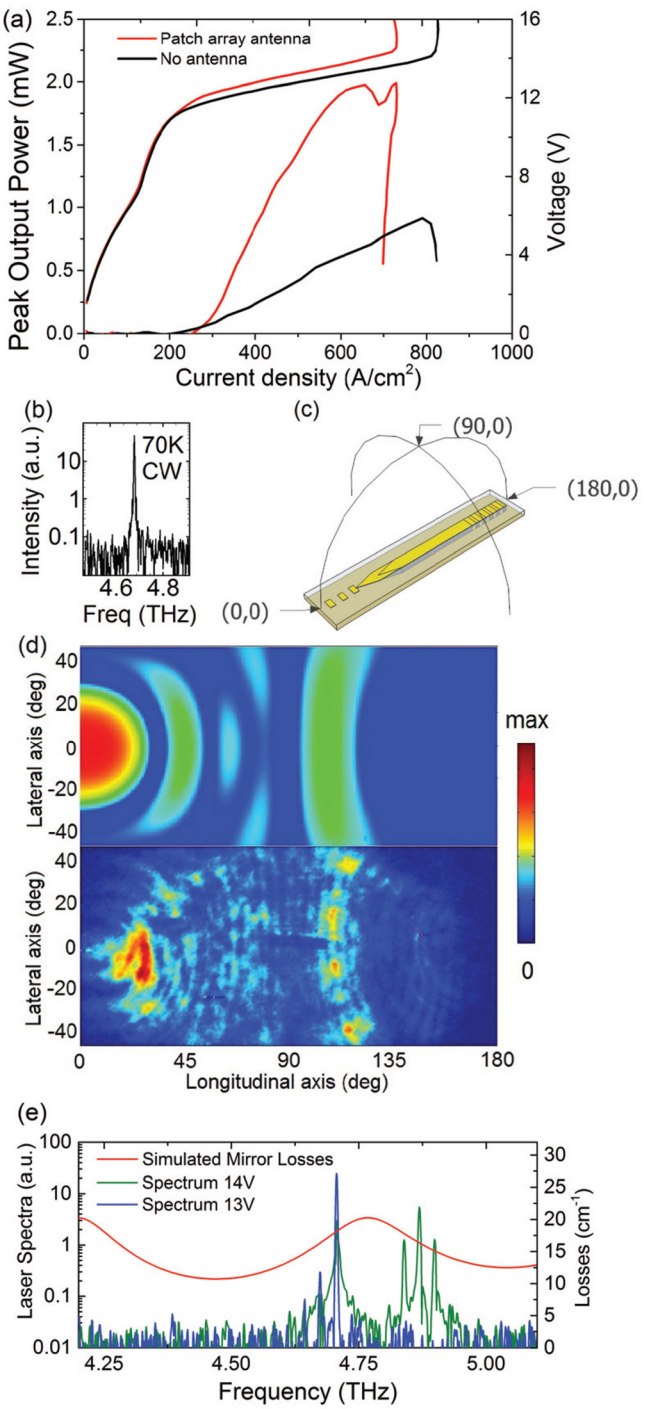

FIG. 3. (a) Comparison between pulsed LIVs of the patch array antenna device and an antennaless one. The power was measured in front of the facet with a Thomas Keating detector. The device was pumped with 150 ns pulses at 10% duty-cycle. (b) Spectrum of the slot array antenna device at 70 K operated in CW. (c) Schematic drawing of the angles used to represent the far-field measurements. (d) Comparison between the computed patch array antenna far-field at 4.67 THz and measured far-field at 377 A/cm^2. (e) Spectra of the slot array antenna at 13 and 14 V together with the computed mirror losses from the antenna.

The measurement of the far-field shown in Figure 3(d) with the angles defined in (c) was done at a pumping current of 513 A/cm^2, where more than 91% of the power is contained in the mode at 4.67 THz. The main features of the experimental farfield: the bright spot to the front as well as the shallower and wider arc at 110° on the longitudinal axis are well reproduced by simulation. In addition, no field is emitted by the laser backwards, which shows the correct operation of the Bragg reflector. The difference between the predicted and measured farfield is attributed reflections occurring on the cryostat.

TABLE I. Comparison between the patch array antenna and an antennaless device.

Antenna	$J_{threshold}$ (A/cm^2)	Slope efficiency (mW/A)	Max peak power (mW)
Without	240	4.5	0.9
Patch array	281	18.4	2

The slot array antenna device shows a similar behavior, summarised in Table II. The laser operated at a temperature above 100 K with 150 ns pulses and 10% duty cycle and up to 70 K in continuous wave as shown in Figure 3(b). The reflectivity from the antenna and impedance matching element is measured to be 1.5% where it was computed to 1.1%.

In addition, the laser emission spectrum switches from single mode to multimode in the range of 4.65–4.9 THz with a mode spacing of 29.9 GHz corresponding to the free spectral range of the Fabry-Perot formed between the antenna and the Bragg mirror. This shows that the impedance matching element has a sufficiently low reflectivity to avoid feedback. We assumed a group refractive index of 4.2 for the amplifier section waveguide. This value is significantly higher than the refractive index of the active region at 3.75, due to the increasing material dispersion from the bulk Gallium Arsenide close to the longitudinal optical phonons frequency at 8.7 THz.

The effect of the slot array antenna can be seen in its emission spectrum shown in Figure 3(e). It shows a gap around 4.78 THz, the point of highest antenna losses of the simulated structure.

In conclusion, we have demonstrated a facet reflectivity control for double metal waveguide THz QCLs. Integrated planar slot and patch array antennas on BCB were used as an outcoupling element and a Bragg mirror as a highly reflective element. The effects of the antennas were confirmed by the threshold current and onset of the negative differential resistance, the slope efficiency, the maximum peak output power, the spectra, and the far-field of the laser. This work paves the way to an antenna coupled external cavity double metal THz QCL.

Many thanks to Dana Turcinkova and Zhaolu Diao for their advices in terms of processing. The devices were realized in FIRST Center for Micro- and Nanoscience. This work was supported by the Swiss National Foundation (SNF) No. 140463 “THz Photonics and Polaritonics” and

TABLE II. Comparison between the slot array antenna and an antennaless device.

Antenna	$J_{threshold}$ (A/cm^2)	Slope efficiency (mW/A)	Max peak power (μW)
Without	257	3.5	400
Slot array	304	9.5	800

carried out within the collaborative research centre 956, funded by the Deutsche Forschungsgemeinschaft.

[1]J. Faist, F. Capasso, D. L. Sivco, C. Sirtori, A. L. Hutchinson, and A. Y. Cho, Science **264**, 553 (1994).
[2]R. Kohler, A. Tredicucci, F. Beltram, H. E. Beere, E. H. Linfield, A. G. Davies, D. A. Ritchie, R. C. Iotti, and F. Rossi, Nature **417**, 156 (2002).
[3]C. Walther, G. Scalari, M. I. Amanti, M. Beck, and J. Faist, Science **327**, 1495 (2010).
[4]G. Scalari, C. Walther, M. Fischer, R. Terazzi, H. Beere, D. Ritchie, and J. Faist, Laser Photon. Rev. **3**, 45 (2009).
[5]B. S. Williams, Nature Photon. **1**, 517 (2007).
[6]M. A. Belkin, J. A. Fan, S. Hormoz, F. Capasso, S. P. Khanna, M. Lachab, A. G. Davies, and E. H. Linfield, Opt. Express **16**, 3242 (2008).
[7]M. I. Amanti, G. Scalari, R. Terazzi, M. Fischer, M. Beck, J. Faist, A. Rudra, P. Gallo, and E. Kapon, New J. Phys. **11**, 125022 (2009).
[8]J. Faist, *Quantum Cascade Lasers* (Oxford University Press, 2013).
[9]J. Xu, J. M. Hensley, D. B. Fenner, R. P. Green, L. Mahler, A. Tredicucci, M. G. Allen, F. Beltram, H. E. Beere, and D. A. Ritchie, Appl. Phys. Lett. **91**, 121104 (2007).
[10]A. W. M. Lee, Q. Qin, S. Kumar, B. S. Williams, Q. Hu, and J. L. Reno, Opt. Lett. **32**, 2840 (2007).
[11]M. I. Amanti, M. Fischer, C. Walther, G. Scalari, and J. Faist, Electron. Lett. **43**, 573 (2007).
[12]A. A. Tavallaee, P. W. C. Hon, Q. S. Chen, T. Itoh, and B. S. Williams, Appl. Phys. Lett. **102**, 021103 (2013).
[13]H. A. Wheeler, IEEE Trans. Antennas Propag. **Ap23**, 462 (1975).
[14]L. J. Chu, J. Appl. Phys. **19**, 1163 (1948).
[15]Z. L. Diao, C. Bonzon, G. Scalari, M. Beck, J. Faist, and R. Houdre, Laser Photon. Rev. **7**, L45 (2013).
[16]See supplementary material at http://dx.doi.org/10.1063/1.4871369 for a discussion on the simulation parameters.
[17]E. Perret, N. Zerounian, S. David, and F. Aniel, Microelectron. Eng. **85**, 2276 (2008).
[18]M. I. Amanti, M. Fischer, G. Scalari, M. Beck, and J. Faist, Nature Photon. **3**, 586 (2009).
[19]H. Zhang, G. Scalari, M. Beck, J. Faist, and R. Houdre, Opt. Express **19**, 10707 (2011).
[20]M. Martl, J. Darmo, C. Deutsch, M. Brandstetter, A. M. Andrews, P. Klang, G. Strasser, and K. Unterrainer, Opt. Express **19**, 733 (2011).
[21]G. Scalari, R. Terazzi, M. Giovannini, N. Hoyler, and J. Faist, Appl. Phys. Lett. **91**, 032103 (2007).